

Note: This copy is for your personal, non-commercial use only. To order presentation-ready copies for distribution to your colleagues or clients, use the *Radiology Reprints* form at the end of this article.

Detector or System? Extending the Concept of Detective Quantum Efficiency to Characterize the Performance of Digital Radiographic Imaging Systems¹

Ehsan Samei, PhD
Nicole T. Ranger, MSc
Alistair MacKenzie, MSc
Ian D. Honey, MSc
James T. Dobbins III, PhD
Carl E. Ravin, MD

Purpose:

To develop an experimental method for measuring the effective detective quantum efficiency (eDQE) of digital radiographic imaging systems and evaluate its use in select imaging systems.

Materials and Methods:

A geometric phantom emulating the attenuation and scatter properties of the adult human thorax was employed to assess eight imaging systems in a total of nine configurations. The noise power spectrum (NPS) was derived from images of the phantom acquired at three exposure levels spanning the operating range of the system. The modulation transfer function (MTF) was measured by using an edge device positioned at the anterior surface of the phantom. Scatter measurements were made by using a beam-stop technique. All measurements, including those of phantom attenuation and estimates of x-ray flux, were used to compute the eDQE.

Results:

The MTF results showed notable degradation owing to focal spot blur. Scatter fractions ranged between 11% and 56%, depending on the system. The eDQE(0) results ranged from 1%–17%, indicating a reduction of up to one order of magnitude and different rank ordering and performance among systems, compared with that implied in reported conventional detective quantum efficiency results from the same systems.

Conclusion:

The eDQE method was easy to implement, yielded reproducible results, and provided a meaningful reflection of system performance by quantifying image quality in a clinically relevant context. The difference in the magnitude of the measured eDQE and the ideal eDQE of 100% provides a great opportunity for improving the image quality of radiographic and mammographic systems while reducing patient dose.

© RSNA, 2008

¹ From the Duke Advanced Imaging Laboratories, Department of Radiology, Duke University and Medical Center, 2424 Erwin Rd (Hock Plaza), Suite 302, Durham, NC 27705 (E.S., N.T.R., J.T.D., C.E.R.); and King's College for the Assessment of Radiological Equipment, Department of Medical Engineering and Physics, King's College Hospital, London, England (A.M., I.D.H.). Received October 1, 2007; revision requested December 18; revision received May 20, 2008; accepted May 29; final version accepted May 30. Supported in part by National Institutes of Health grants R01 CA80490 and R01 CA109074. **Address correspondence** to N.T.R. (e-mail: nicole.ranger@duke.edu).

Image quality is an important attribute of an imaging system, as it can have a measurable effect on the diagnostic utility and clinical usability of a system. To ensure sufficient and consistent performance, it is necessary to be able to assess image quality quantitatively so that it can be optimized and monitored to maintain a high level of clinical care. In the past few years, the most recognized and comprehensive metric of image quality performance for digital radiographic and mammographic systems has been the detective quantum efficiency (DQE), a measure of the efficiency of a detector when using the input signal-to-noise ratio (SNR) provided by a limited number of x-ray photons to form an image at a certain exposure or dose level. With measurement methods largely standardized (1–5), a number of studies have reported the variations in DQE performance of these imaging systems (6–9).

While the DQE provides a quantitative measure of image quality per unit of exposure to the detector, it does not include some important attributes of the total system that affect the quality of images captured clinically. Clinical images are affected by the presence of scattered radiation, the attenuation properties of the commonly used antiscatter grids, and the blur caused by the finite size of the focal spot (10,11). The current measurement techniques for assessing the DQE are devised to eliminate or minimize those factors so that the result will be reflective of the perfor-

mance of the image detector alone. As such, the DQE measure remains largely an engineering or academic specification for the detector, with limited clinical applicability since it does not represent the performance of the system as a whole. Some excellent work has already been done to develop the theoretical framework for an expanded concept of DQE to include factors other than the detector (12–17). However, as of yet, no large-scale evaluation of commercially available systems has been conducted by using this method, to our knowledge.

We recently developed an experimental method to quantitatively assess the performance, as it relates to image quality, of a digital radiographic system in the presence of scattered radiation, an antiscatter grid, magnification, and focal spot blur (18). This method involved the measurement of the DQE in the presence of these additional system attributes to determine an effective DQE (eDQE), which would be applicable to the overall imaging system, as opposed to the detector only. As such, the eDQE provides a measure of actual image quality (ie, image SNR) per unit of incident exposure (and by inference, dose level) to the patient. This study involved an evaluation of the use of this experimental method when applied to a number of commercially available digital radiographic imaging systems.

Materials and Methods

For unrelated projects, one of the authors (J.T.D.) has received research funding from and has been an invited speaker at scientific events sponsored by GE Healthcare (Milwaukee, Wis) and another (E.S.) has served as a consultant for Siemens Medical Solutions (Malvern, Pa). These relationships had no bearing on the current study, the study authors had full control of the data and the information submitted for publication, and there was no review of the manuscript by any commercial entity.

Phantom

The study employed a phantom designed by the Food and Drug Adminis-

tration for use in the Nationwide Evaluation of X-ray Trends program, which monitors radiographic exposures at clinical facilities across the United States (19,20). The phantom, which emulates the attenuation and scatter conditions encountered in chest radiography, is well established and has been in use for many years. The adult version of the phantom used in this study consists of 25.4×25.4 -cm slabs of acrylic and aluminum, separated by an air gap that emulates the thoracic cavity. It also includes a stand for the placement of an ionization chamber in the beam to provide consistent measurement of in-air exposure during an image acquisition and a supplemental insert for the measurement of limiting resolution, which was not used in this study. Figure 1 provides a side-view schematic of the phantom that shows its geometry and composition.

Imaging Systems

A total of seven digital radiographic imaging systems were evaluated in the study. Table 1 summarizes the basic specifications of the systems and the operating modes and techniques under which the systems were tested. The systems represented a wide range of detector technologies, including computed

Advances in Knowledge

- To develop an experimental method for measuring the effective detective quantum efficiency of digital radiographic imaging systems that characterizes system performance in a clinically realistic context, reflecting the effect on performance from x-ray scatter, magnification, focal spot blurring, and the use of an antiscatter grid.
- To evaluate the use of this experimental method in a select group of digital chest radiographic imaging systems.

Published online

10.1148/radiol.2492071734

Radiology 2008; 249:926–937

Abbreviations:

CCD = charged-coupled device
 DQE = detective quantum efficiency
 eDQE = effective DQE
 MTF = modulation transfer function
 NPS = noise power spectrum
 NNPS = normalized NPS
 SNR = signal-to-noise ratio

Author contributions:

Guarantors of integrity of entire study, all authors; study concepts/study design or data acquisition or data analysis/interpretation, all authors; manuscript drafting or manuscript revision for important intellectual content, all authors; approval of final version of submitted manuscript, all authors; literature research, E.S., N.T.R., A.M., I.D.H., J.T.D.; experimental studies, E.S., N.T.R., A.M., I.D.H.; statistical analysis, E.S., N.T.R.; and manuscript editing, all authors.

See Materials and Methods for pertinent disclosures.

radiographic, indirect flat-panel, direct flat-panel, full-field charged-coupled device (CCD)-based, and slot-scan CCD-based detectors.

All systems were tested under operating conditions representative of those used clinically. Those conditions included the choice of grid, operating kilovolt peak levels, and the size of the focal spot. As such, some systems were tested in multiple operating modes. Overall, the systems were evaluated in a total of nine operating modes (Table 1). All systems were calibrated according to the manufacturer's protocol and were in clinical use at the time of evaluation.

Following image acquisition, detailed below, the image data were transferred to a central computer for analysis. All image data were analyzed in the "for processing" format, with gain and offset, bad pixel, and geometric distortion calibrations applied (when applicable) but otherwise without any additional postprocessing. For all systems, this transformation yielded a generalized relationship between pixel values and exposure that was calculated with the equation $Q' = 4000 \times E$, where the image data (Q) were transformed to Q' values that were linearly proportional to

exposure (E), assuming a zero offset, enabling a consistent representation of image data across all systems. This rescaling and linearization was performed on the basis of the system re-

sponse function that defines the relationship between pixel values and incident exposure. This function was measured for each system, following a method similar to that reported previ-

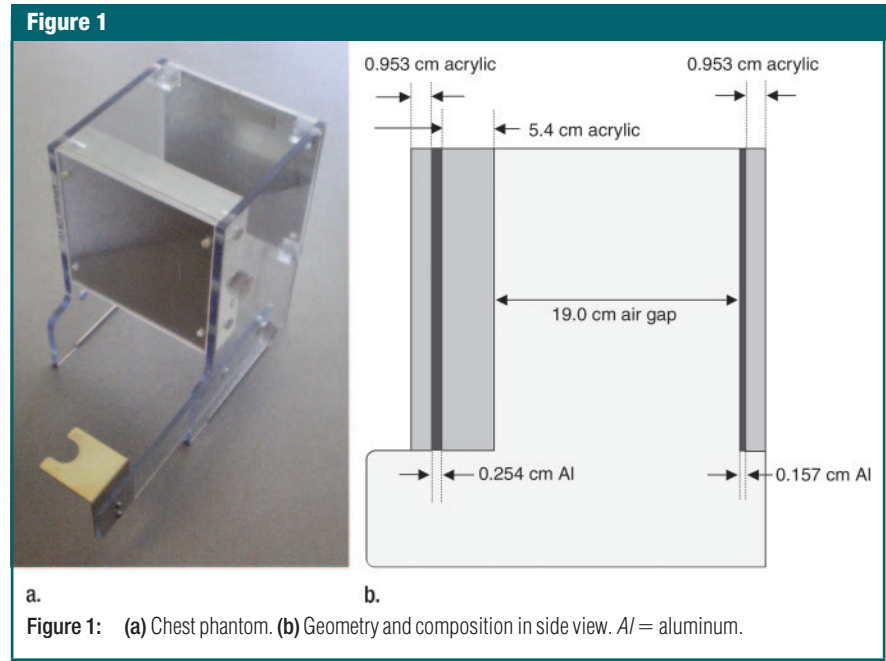


Table 1

Basic Specification of Imaging Systems Tested in the Study

System and Manufacturer	Technology	Pixel Size (mm)	Grid Type (In/cm) and Ratio	Beam Quality (kV)	Nominal Focal Spot Size (mm)	Source-to-Image Distance (cm)	Exposure Levels for $E_0/3.2, E_0$, and $3.2E_0$ (mR)*
Revolution xQ/i (GE Healthcare, Milwaukee, Wis)	aSi:Csl Indirect flat-panel	0.2	Stationary, 78; 13:1	120	1.2	180	1.8 (15.7), 5.6 (48.8), 18.4 (160.4)
Axiom Aristos (Siemens Medical Solutions, Forchheim, Germany)	aSi:Csl Indirect flat-panel	0.143	Stationary, 80; 15:1	121 (0.1 mm Cu)	1.25, 0.6	180	1.7 (14.8), 3.2 (27.9), 9.9 (86.3)
CXDI-40G (Canon Medical Systems, Lake Success, NY)	aSi:GOS Indirect	0.160	Stationary, 40; 10:1	120	1.0	180	2.1 (18.3), 5.6 (48.8), 16.2 (141.3)
Compact+ (Agfa, Leverkusen, Germany)	Computed radiography	0.15	None used	81	1.0	157	1.7 (14.8), 5.3 (46.2), 16.1 (140.4)
			Moving, 70; 17:1	121		180	3.4 (29.6), 9.7 (84.6), 30.7 (267.7)
Xplorer 1500 (Imaging Dynamics, Calgary, Canada)	Full-field CCD-based	0.108	Stationary, 70; 13:1	121	1.2	180	3.0 (26.2), 9.3 (81.1), 29.6 (258.1)
EPEX (Hologic, Bedford, Mass)	aSe Direct flat-panel	0.139	Stationary, 70; 10:1	122	1.2	180	3.1 (27.0), 9.0 (78.5), 27.4 (238.9)
ThoraScan (Delft Imaging Systems, Veenendaal, the Netherlands)	Slot-scan CCD-based	0.155	None used	140	1.3	173	2.6 (22.7), 8.5 (74.1), 26.4 (230.2)

Note.—All systems were evaluated with the grid used in routine clinical chest examinations. aSe = amorphous selenium, aSi = amorphous silicon, Csl = cesium iodide, GOS = gadolinium oxysulfide.

* Values reflect free-in-air measurements inverse-square corrected to the detector surface. Values in parentheses are air kerma values, measured in micrograys.

Figure 2

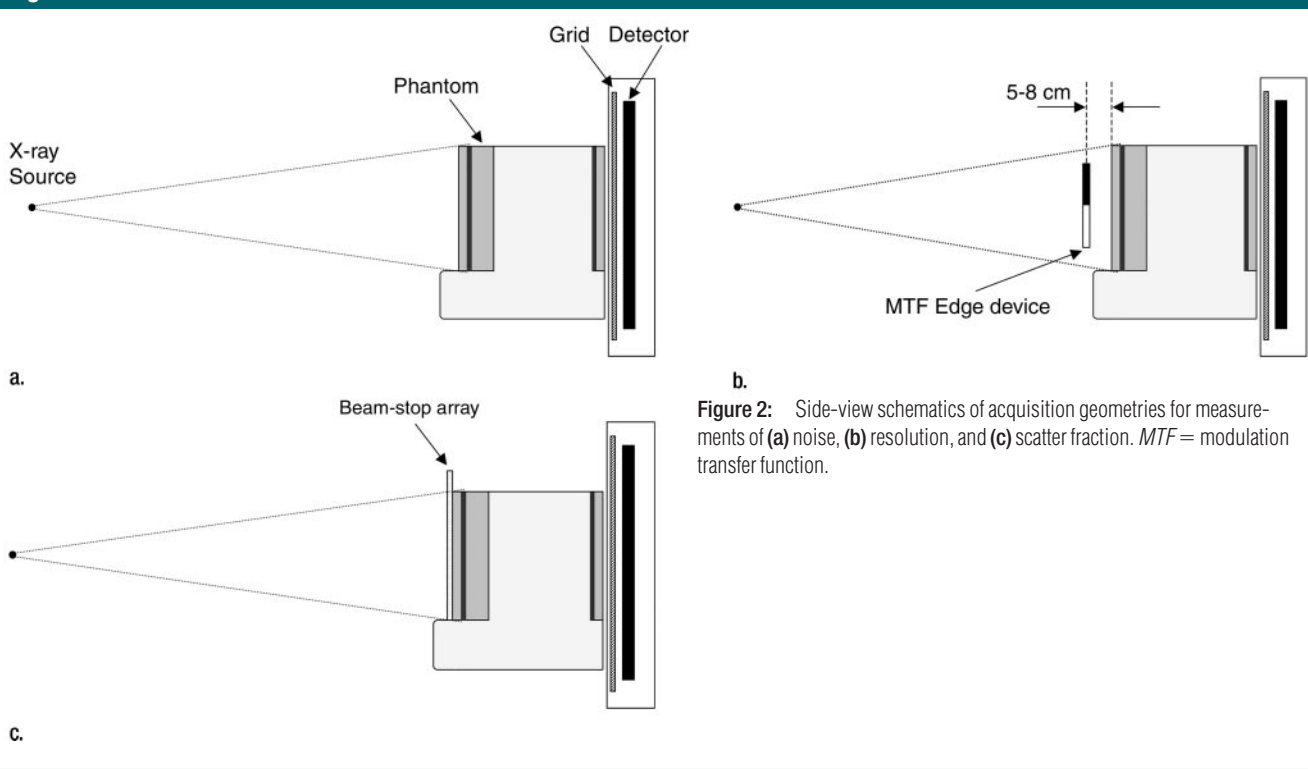


Figure 2: Side-view schematics of acquisition geometries for measurements of (a) noise, (b) resolution, and (c) scatter fraction. *MTF* = modulation transfer function.

Table 2

Ideal SNRs, Measured Scattered Fractions, and Photon Transmission Fractions of the Systems Tested in the Study

System and Manufacturer	Grid Type, Line Density (lines/cm), and Grid Ratio	Beam Quality (kV)	q Value (mR ⁻¹ , mm ⁻²)	Relationship between Pixel Value (<i>Q</i>) and Exposure (<i>E</i>)*	Scatter Fraction (%)	Phantom Transmission Fractions (%) [†]
Revolution xQ/i (GE Healthcare, Milwaukee, Wis)	Stationary, 78; 13:1	120	255, 100	$Q = 845.2E + 11.3$ ($R^2 = 1.000$)	33.0	10.3 narrow 17.5 wide
Axiom Aristos (Siemens Medical Solutions, Malvern, Pa)	Stationary, 80; 15:1	121 (0.1mm Cu)	262, 885	$Q = -776.2E + 4083.3$ ($R^2 = 1.000$)	32.7	12.6 narrow 22.0 wide
CXDI-40G (Canon Medical Systems, Lake Success, NY)	Stationary, 40; 10:1	120	255, 100	$Q = 367.6 \ln E + 2710.3$ ($R^2 = 1.000$)	31.4	9.7 narrow 17.5 wide
Compact+ (Agfa, Leverkusen, Germany)	None used	81	235, 648	$Q = 524.5 \ln E + 2626.4$ ($R^2 = 1.000$)	55.6	6.6 narrow 12.0 wide
	Moving, 70; 17:1	121	255, 100	$Q = 539.8 \ln E = 2757.9$ ($R^2 = 1.000$)	26.8	10.0 narrow 17.5 wide
Xplorer 1500 (Imaging Dynamics, Calgary, Canada)	Stationary, 70; 13:1	121	255, 100	$Q = 511.5E - 4.7$ ($R^2 = 0.9999$)	49.7	9.6 narrow 17.5 wide
EPEX (Hologic, Bedford, Mass)	Stationary, 70; 10:1	120	255, 100	$Q = 596.6 \ln E + 2038.2$ ($R^2 = 0.9993$)	38.1	9.8 narrow 17.5 wide
ThoraScan (Delft Imaging Systems, Veenendaal, the Netherlands)	None used	140	252, 205	$Q = -430.7E + 4098.7$ ($R^2 = 0.9995$)	10.7	10.7

* R^2 is the square of the correlation coefficient; *E* was measured in milliroentgens.

[†] Narrow-beam transmission values were used for eDQE computations. The wide-beam values, reported here as reference, were measured with the beam covering the full detector and the ionization chamber placed 5 cm from exit surface of the phantom (emulating the typical air gap between detector and outer cover). For the ThoraScan system, only a single beam type was used with the ionization probe placed at 9.3 cm from the exit surface of the phantom by using the slot-scan fan beam used in chemical imaging.

Figure 3

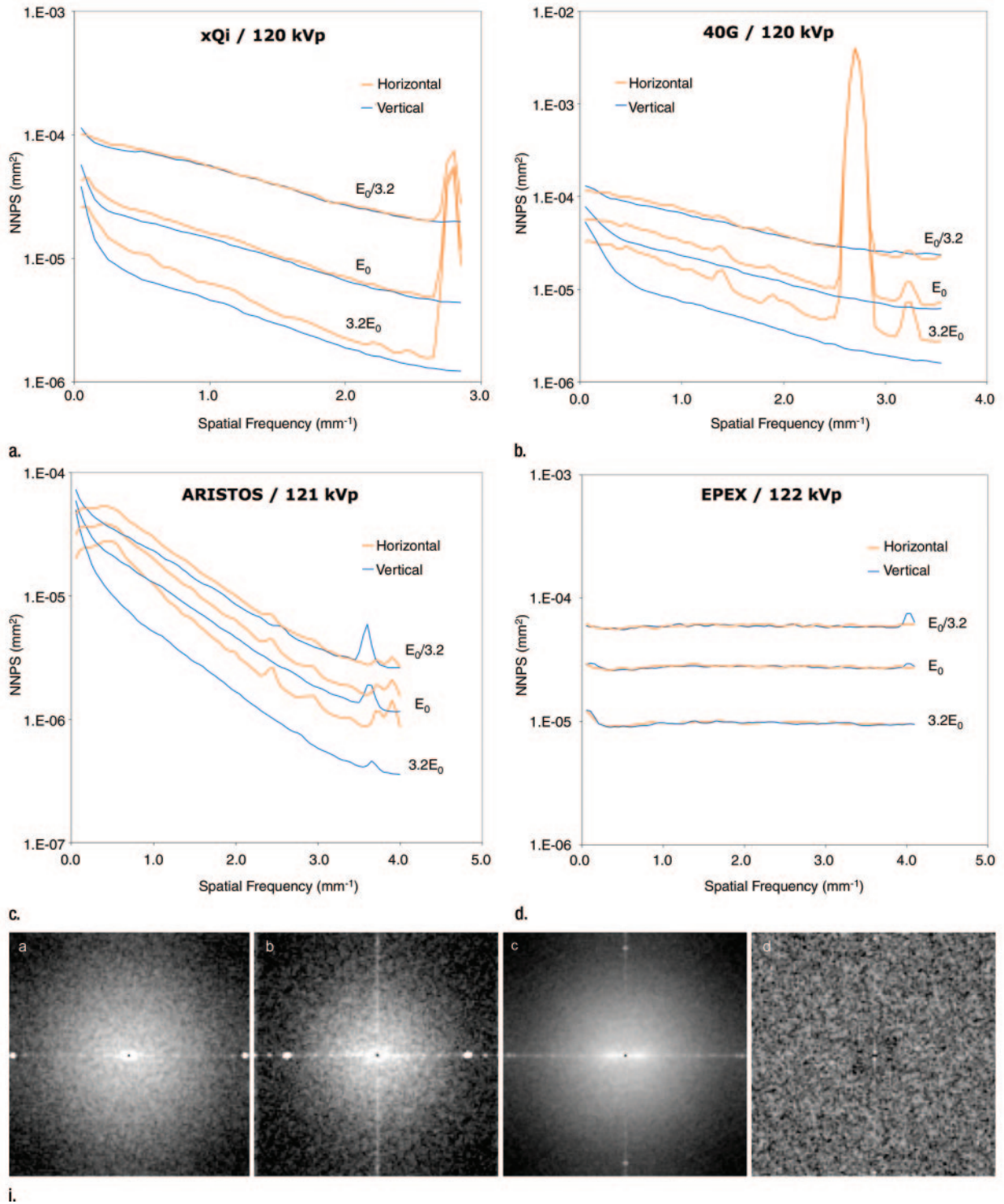
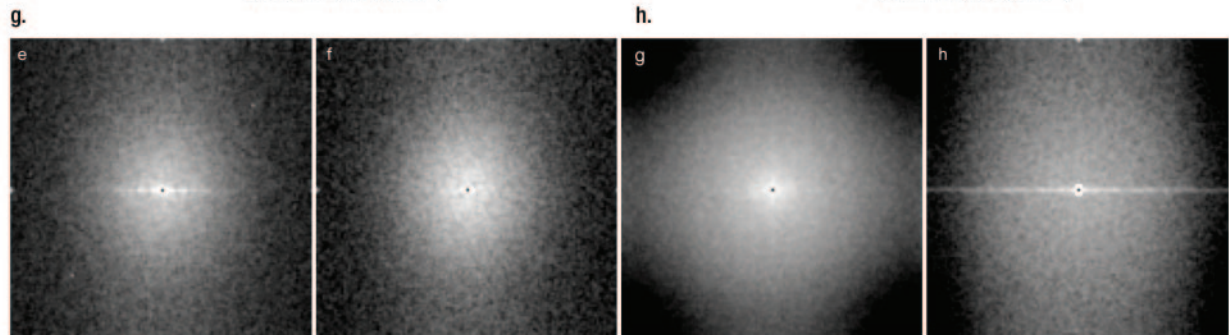
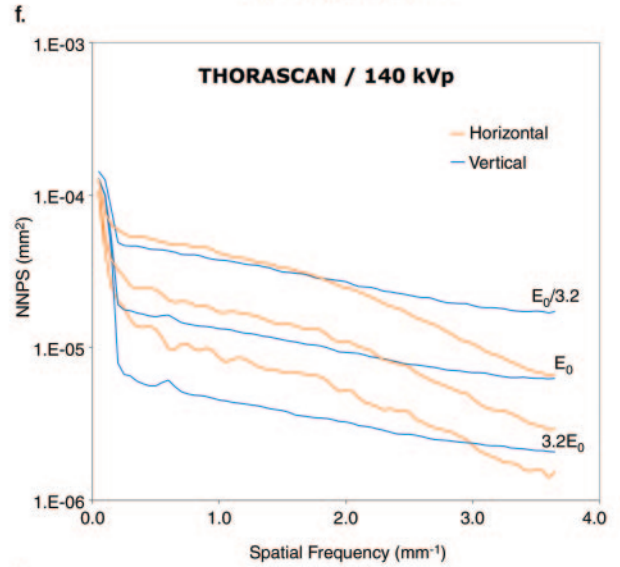
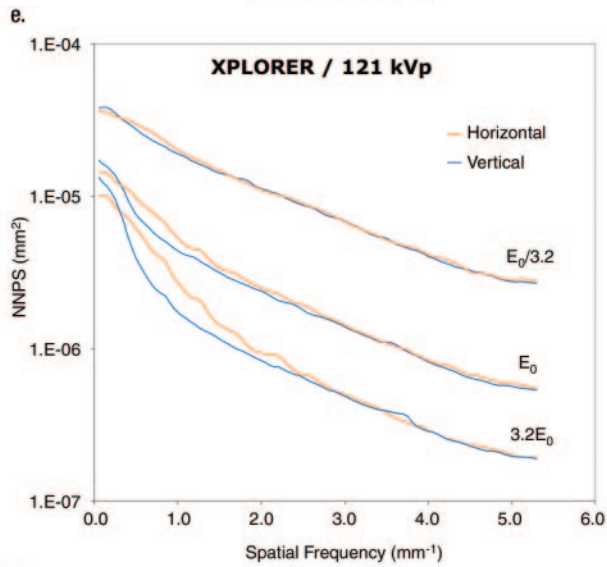
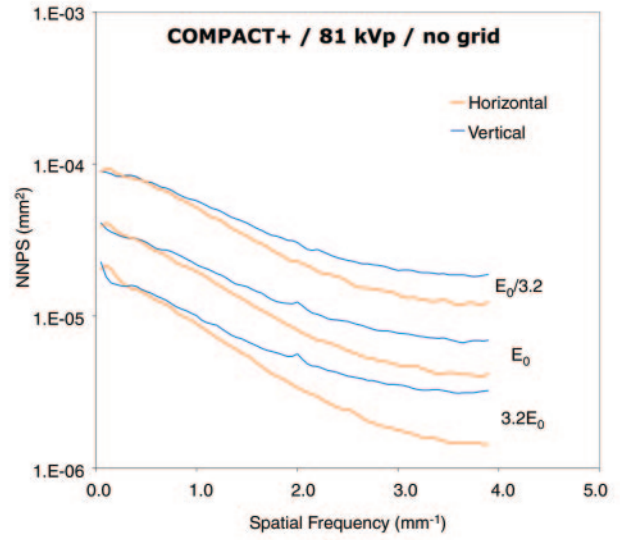
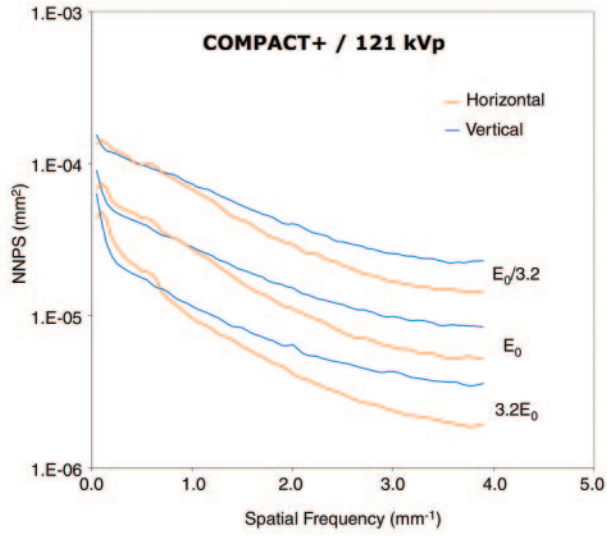


Figure 3: (a–h) NNPS of systems in orthogonal directions at three evaluated exposure levels, where E_0 is target operating exposure (Table 1). (i) Two-dimensional NPS for eight configurations represented in a–h are also shown. (Fig 3 continues.)

Figure 3 (continued)



i.
Figure 3 (continued)

ously (2), but with the phantom placed in proximity to the x-ray source in lieu of the additional filtration required by the International Electrotechnical Commission standard (4).

Noise Measurements

The noise properties of the systems in the nine operating modes of Table 1 were measured by using the image acquisition set-up illustrated in Figure 2a. The phantom was placed immediately next to the detector cover plate. No additional test device was placed in the beam. Images of the phantom were obtained at the applicable beam quality at three exposure levels corresponding to $E_0/3.2$, E_0 , and $3.2E_0$, where E_0 is the exposure at which a system is normally operated. The choice of this range of exposures was inspired by the concept of a normal level of exposure, as defined by the International Electrotechnical Commission standard (4). The tube current–time product (measured in milli-ampere seconds) setting needed to establish the target E_0 value was determined (a) by using a photo-timed image acquisition that used the phantom or (b) from technique charts used in routine clinical operation of the system. Exposures were measured free in air by using a 10×5 –6 calibrated ionization chamber (MDH 1015 or 2025; Radcal, Monrovia, Calif). At each exposure condition, repeated images were captured to obtain at least 4 000 000 independent pixels within a central analysis area corresponding to 18×18 cm.

The acquired linearized images were processed to deduce the noise power spectrum (NPS). The processing followed established steps, including the division of the central 18×18 -cm area of each image into sequential 128×128 -pixel regions of interest, detrending of the data, the division of the data by their mean value, the determination of the normalized NPS (NNPS) for each region of interest by using Fourier transformation, the averaging of the NNPS values from the regions of interest from all repeat images, and deducing the directional NNPS by using band averaging. The details of these steps are well described in the literature (2,21).

Figure 4

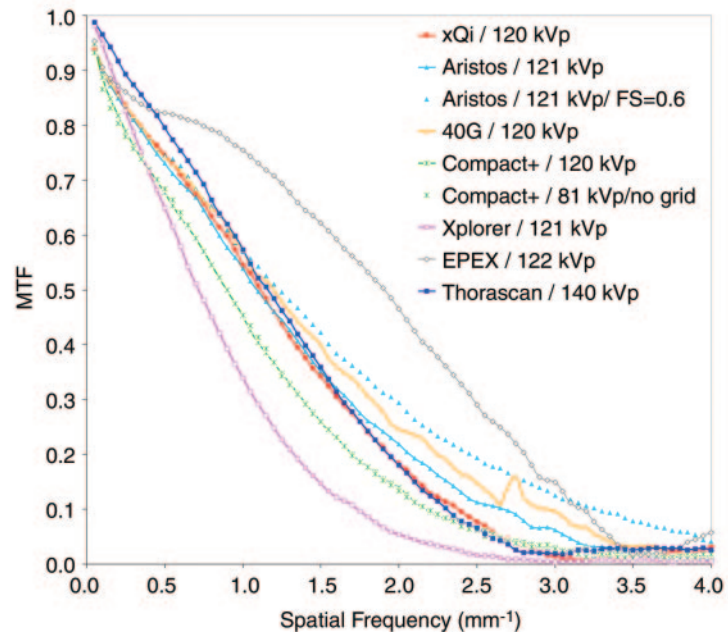


Figure 4: MTF results in horizontal direction across different systems at comparable beam quality.

Resolution Measurements

The resolution of the systems in the nine operating modes (Table 1) was also measured. The image acquisition set-up is illustrated in Figure 2b. The phantom was placed immediately next to the detector cover plate. An opaque edge test device (TX5; Scanditronix-Wellhöffer, Schwarzenbruck, Germany) was placed at the center of the beam, approximately 5–8 cm from the anterior surface of the phantom. The edge was oriented vertically. The location of the edge test device enabled the measurement of the system resolution in the presence of focal spot blur penumbra, magnification, scattered radiation, and the antiscatter grid (when applicable). Three images of the edge test device were then captured at the applicable beam quality at an exposure of $3E_0$.

The acquired images, once linearized as previously described, were processed to deduce the MTF. The processing followed established steps, including the extraction of the edge region of interest, the determination of the edge angle and location in the image, the determination of the edge and line spread functions, and the deduction of the MTF

by using Fourier transformation. The MTFs from three repeat images were averaged. The details of these steps are well described in the literature (1,22).

Scatter Measurements

The scatter properties of the systems in the nine operating modes (Table 1) were measured by using a beam-stop array device (23,24) placed adjacent to the anterior surface of the phantom (Figure 2c). The phantom was centered in the field of view and adjacent to the detector cover plate. The beam-stop array device was composed of a 14×16 array of 224 lead cylinders, each of which was 6 mm thick, 3 mm in diameter, spaced 25 mm apart, and embedded in a 6-mm-thick sheet of polystyrene. Three images of the device were captured by using the applicable beam quality at an exposure of $3E_0$.

The acquired images were linearized prior to deducing the scatter fraction. The average scatter fraction was computed across 20 beam stops at the center of the image by using the measurement of mean pixel values within a 10×10 -pixel region of interest positioned over each beam stop, divided by the average of mean pixel

values in regions of interest on either side of the beam stop.

Estimation of the eDQE

Incorporating the influence of scatter, magnification, grid, and focal spot blur, the effective DQE for each system was estimated by using the measured MTF and NPS, the incident exposure, the ideal squared SNR per unit of exposure (q), and narrow-beam phantom transmission

fraction, measured at the applicable beam qualities (18). In this formulation, the detector-grid-cover combination was treated as a unit, penalizing the system for grid and cover attenuation, but not for phantom attenuation. The values for q , tabulated in Table 2, were estimated for an ideal counting detector and the applicable x-ray spectrum transmitted through the phantom (assuming only the primary beam), by using a radiographic simulation

routine (21) (xSpect; Henry Ford Hospital, Detroit, Mich).

Results

Overall, all systems that were tested demonstrated excellent linearity. The pixel values were linearly proportional to exposure or to the logarithm of exposure. The equations describing those relationships are denoted in Table 2,

Figure 5

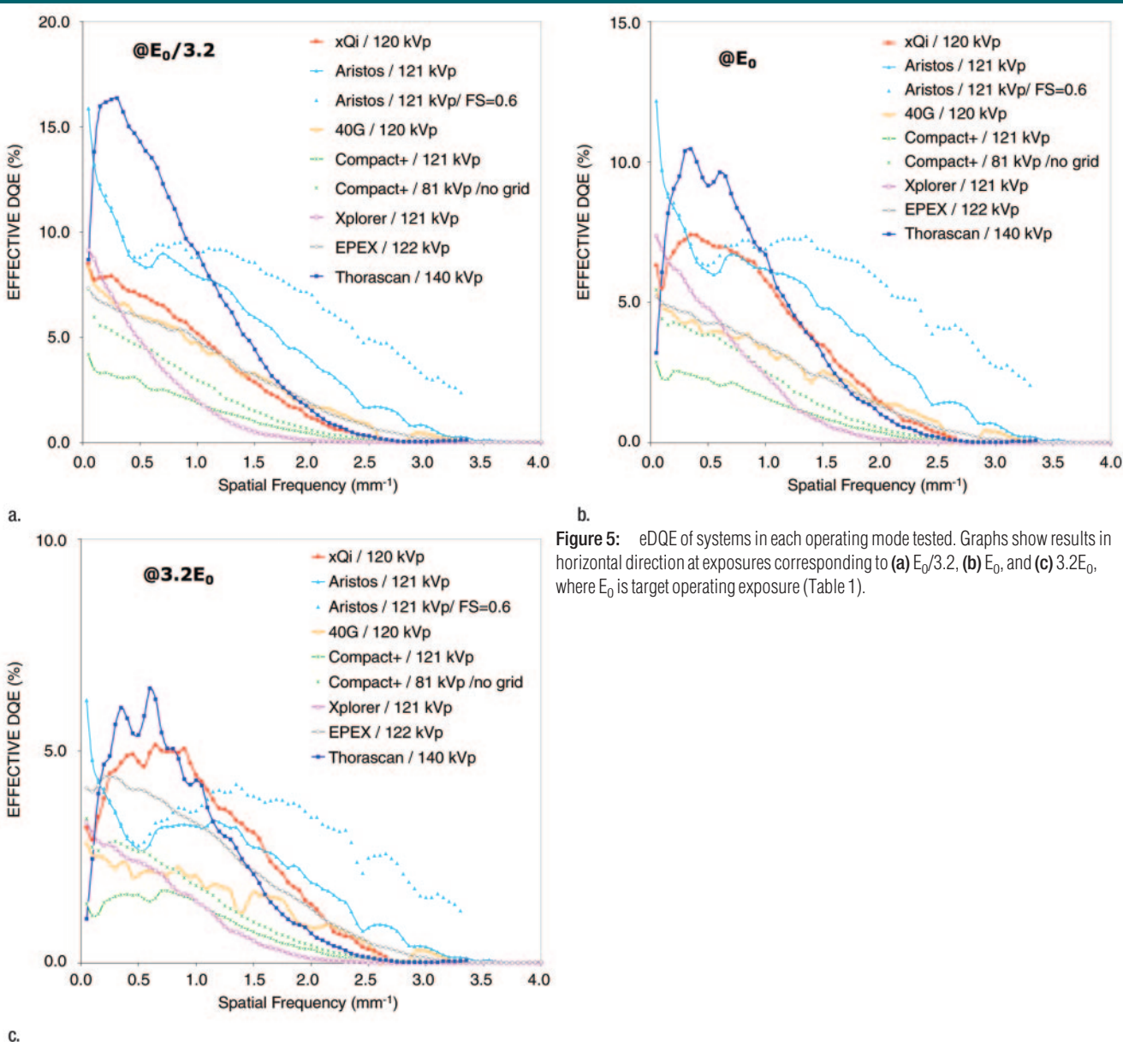


Figure 5: eDQE of systems in each operating mode tested. Graphs show results in horizontal direction at exposures corresponding to (a) $E_0/3.2$, (b) E_0 , and (c) $3.2E_0$, where E_0 is target operating exposure (Table 1).

along with the square of the correlation coefficient of the fits (R^2). The R^2 values ranged between 0.9993 and 1.0.

Noise

Figure 3 illustrates the results of the NNPS measurements on the systems in the horizontal and vertical directions at the three exposure levels of $E_0/3.2$, E_0 , and $3.2E_0$. The results for the system with the use of a small focal spot are not reported here, as they were similar to those obtained with the use of a larger focal spot.

For most systems with a stationary grid, the magnitude of the NNPS is greater in the direction perpendicular, rather than parallel, to the grid lines (here, corresponding to the horizontal and vertical directions, respectively), particularly at higher exposure levels. This may be attributed to the grid structure associated with the orientation of the grid lines (18). As the exposure increases, this structure constitutes a relatively larger component of the total image noise, reflected here in increased horizontal NNPS. There are also artifacts in the NNPS at specific frequencies related to the grid line spacing (18).

The three exceptions to the above finding are noted for the computed radiographic, CCD-based, and direct flat-panel systems. The computed radiography system used a moving grid; thus, the grid contribution to total noise was diminished owing to spatial averaging of the spatially stochastic grid noise. The magnitude of the horizontal NNPS is also lower for this system owing to the application of anti-aliasing filters to overcome aliasing artifacts associated with data sampling in the horizontal direction (21,25). The slot-scan CCD system does not use a grid and thus has no grid noise. The differences between the horizontal and vertical NNPS findings at low exposure may result from image lag, enhancing the noise in the vertical direction (26). At higher exposures, the noise attributes are further affected by structured nonuniformities in the horizontal direction (26). Those nonuniformities similarly contribute to the NNPS findings from the full-field CCD-based system. For the direct flat-panel system, the horizontal and vertical NNPS findings are identical,

Figure 6

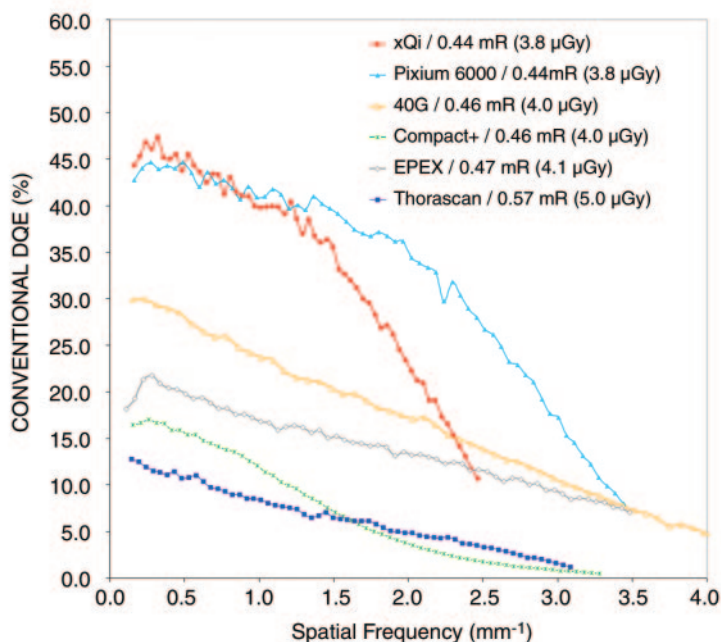


Figure 6: Reported conventional DQE values for selected detectors.

demonstrating noise aliasing that is typical of these devices. The noise properties of the CCD-based and direct systems suggest an effective removal of the noise structure associated with the grid.

Resolution

Figure 4 provides an overall comparison of the MTFs of all the systems when using approximately comparable large focal spots and beam qualities. These different systems, yielding different performances, ranged from the full-field CCD-based system to that of the direct flat-panel detector with its characteristic frequency aliasing (27). The MTFs are naturally reflective of both the limiting spatial resolution performance of the detector, as well as the blur caused by the focal spot magnification. As such, the MTF results reflect the actual resolution that might be obtained when using these systems to perform chest examinations on patients in the clinical setting. The higher the MTF level, the better the performance of the system in depicting fine image details.

Scatter

The scatter fraction results are tabulated in Table 2. Scatter fractions ranged be-

tween 10.7% and 55.6%, depending on the system. Systems with similar grids exhibited similar scatter fraction results. Grids with a higher line density and a higher grid ratio yielded lower scatter fractions. The only two exceptions were the CXDI-40G (Canon Medical Systems; line density, 40 lines/cm; grid ratio, 10:1; scatter fraction comparable to other systems [ie, 31.4%]) and Xplorer 1500 (Imaging Dynamics; line density, grid ratio comparable to majority of systems; unusually high scatter fraction [ie, 49.7%]) systems. These results are likely affected by the unique geometry of these systems (eg, variation in air gap, etc) (28,29), as well as possible contributions from system veiling glare to the measured scatter values (1). The presence of a grid, the use of a lower kilovolt peak level, and a slot-scan acquisition were all associated with a lower scatter fraction measurement, as expected.

eDQE

The eDQE results for each of the nine-system-operating mode combinations is shown in Figure 5. These plots reflect the performance in the horizontal direction at the exposure levels corresponding to

$E_0/3.2$, E_0 , and $3.2E_0$. Overall, the systems show a wide range of performance reflective of the noise, resolution, and scatter components shown earlier. Higher MTFs translate to higher eDQE results at higher spatial frequencies, while peaks in the NPS lead to reductions in the eDQE. For each system, the eDQE decreases with increasing exposure. This is a result of increased influ-

ence of structured noise, which becomes proportionately more influential at higher exposure levels. However, the level of this influence, and thus, the amount of reduction in the eDQE, varies among systems. Therefore, the rank ordering between systems varies with increased exposure.

The most remarkable finding is that the eDQE is lower by an order of magni-

tude than that expected for an ideal system (ie, 100%), even for systems that employ high-DQE detectors; the eDQEs at near-zero frequency ranged from 1%–17%. These results demonstrate how significantly the effects of scatter, magnification, focal spot blur, and grid attenuation, as reflected by the eDQE, can degrade the actual SNR that an imaging system can deliver at a given exposure level in a clinical setting. The ThoraScan (Delft Imaging Systems) system is the exception and does not appear to be much affected by those factors owing to the use of a slot-scan image formation method, which reduces the scatter without the additional primary x-ray attenuation associated with use of an antiscatter grid.

Figure 7

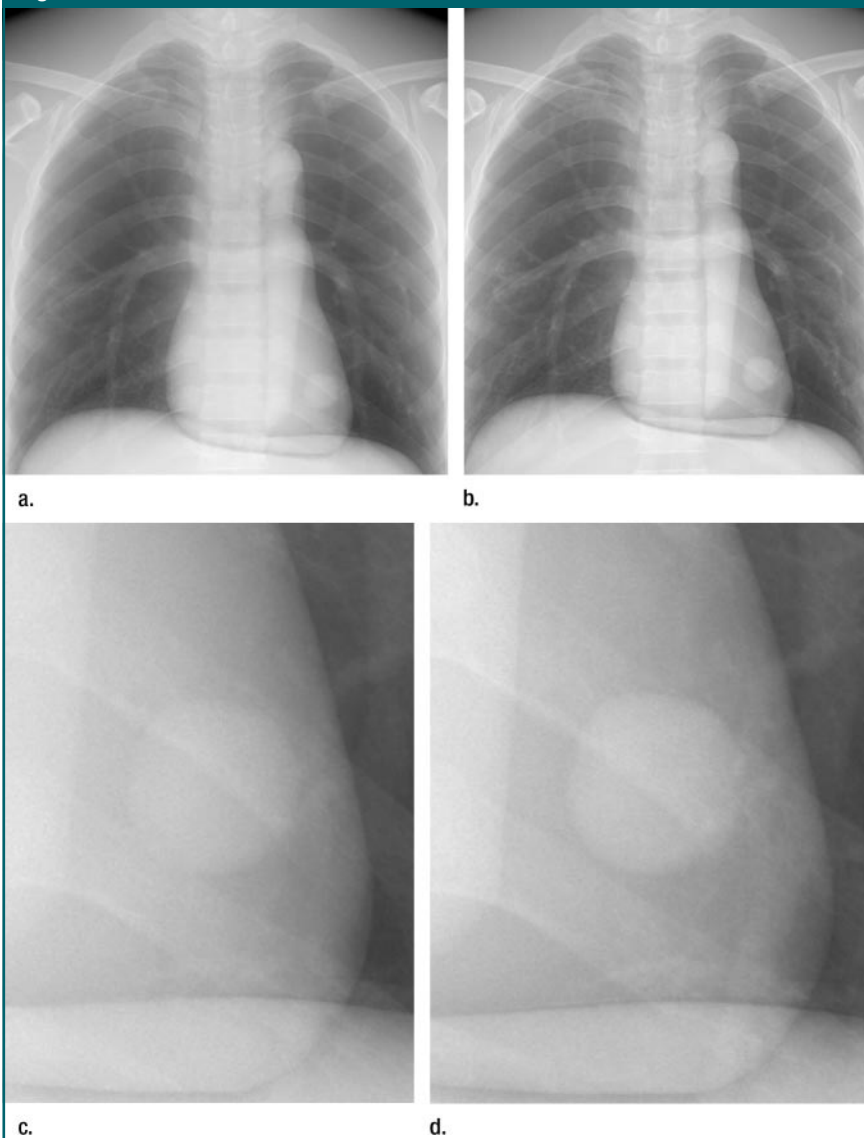


Figure 7: Radiographic images of thoracic phantom acquired with (a, c) xQ/i (GE Healthcare) and (b, d) ThoraScan systems at comparable entrance exposure. ThoraScan system offers improved image quality, with notably lower DQE but higher eDQE than those from xQ/i, demonstrated by improved conspicuity of retrocardiac lesion in d. This shows that eDQE is better metric of system performance than DQE alone.

Discussion

In radiography and mammography, a main goal of image quality measurements is to characterize the performance of imaging systems. Over the years, many techniques have been developed to make such measurements. These techniques have enabled quantitatively accurate and reproducible assessment of the signal and noise properties of imaging detectors, embodied by the universally accepted metric of DQE. However, owing to metrologic constraints, such measurements have focused on the detector alone, ignoring the five substantial attributes of imaging systems that affect image quality: acquisition geometry, scattered radiation, antiscatter grid, magnification, and focal spot blur. If those elements remain consistent, the detector DQE can be used to compare systems. However, those conditions are rarely consistent in clinical implementations of different detectors. Thus, the DQE falls short of reflecting the actual performance of imaging systems in clinical settings where the effects of those attributes are most pronounced.

In this study, we experimentally assessed the performance of radiographic systems in the presence of those attributes by using the eDQE metric (18). The eDQEs of seven digital radiographic imaging systems were measured. The

systems reflected various makes and models in use at different clinical facilities. This metric was found to be easy to measure, while providing a more meaningful reflection of system performance in a clinically relevant context. Our work is the first application of an eDQE to comparatively evaluate a series of commercially available digital radiographic imaging systems.

Our eDQE results indicate that the actual SNR performance for the imaging systems studied is different than that implied by the conventional DQE of the detector alone. A comparison with prior reported DQE results for the detectors might be particularly useful. Figure 6 represents conventional DQE results for some of the tested detectors (7,26). When compared, there is a multifold difference between the DQE results (Fig 6) and the eDQE results (Fig 5), indicating different comparative performance among systems when using DQE, than those represented by the eDQE metric. Most profoundly, the slot-scan system, with a low scatter fraction and no anti-scatter grid, shows a reverse rank ordering relative to full-field systems when comparing the DQE and eDQE results shown in Figures 5 and 6. These findings are consistent with earlier theoretical estimations of eDQE values for that system, given the differences in the phantoms used (23). The relevance of eDQE as a metric of image quality is further demonstrated with the subjective example provided in Figure 7, showing that the ThoraScan system, with a higher eDQE but lower DQE, offers improved conspicuity of a simulated retrocardiac lesion.

These observations suggest that the prevalent comparisons of image quality for digital radiography systems in terms of the DQE alone may need to be revisited. Furthermore, the relative differences in magnitude between the eDQE and DQE, as well as the difference between measured eDQE and the ideal eDQE of 100%, set forth a challenge as well as a great opportunity: There is significant room for improving the image quality of radiographic imaging systems and for reducing patient dose. The largest improvement can be achieved by

using slot-scan image acquisition methods to reduce scatter, and additional improvements could also be achieved with more deliberate use of air gaps. For a fixed exposure time, image resolution can be improved by using air gaps; however, the use of an air gap requires an increased source-to-image distance, an increased detector size, a reduced focal spot size, and increased tube heat loading capacity. The reduced focal spot size by itself can also improve the eDQE response at high spatial frequencies. Improvements can also be achieved in designing better antiscatter grids with reduced primary x-ray attenuation properties.

Notwithstanding the conclusions of the study, certain limitations should be acknowledged. This study employed one geometric chest phantom, which, while reflective of certain typical attributes of digital radiographic imaging of the thorax, is not representative of the range of adult thorax sizes encountered clinically. Furthermore, each radiographic imaging application (eg, mammography, foot, hand, lumbar-spine, etc) would require a different representative phantom; the eDQE is an application-specific metric and thus the conclusions from eDQE results by using a geometric chest phantom cannot be readily extended to other applications. Finally, while a measured eDQE provides a more clinically relevant reflection of the actual SNR performance of an imaging system, it would be important to validate that conclusion by using independent task-specific image quality assessments that included image-based observer studies. Other imaging applications and clinical observer studies remain worthwhile objectives for future studies.

In summary, this study involved a multisystem field trial of eDQE, a metric of image quality, reflecting the actual, clinically relevant SNR performance of a digital radiography system in the presence of x-ray scattering, magnification, focal spot blur, and antiscattering grid. Given our results from a thoracic phantom, there is a multifold difference in the magnitude of the eDQE in comparison with that obtained by using the con-

ventional (detector) DQE method. The eDQE also yields a different relative rank ordering and comparative performance among systems, compared with the conventional DQE. As such, the eDQE metric provides a more meaningful reflection of system performance as it quantifies image quality in a more clinically relevant context.

Acknowledgments: The authors acknowledge the cooperation and help of the personnel at the clinical facilities that allowed use of their equipment: Duke University Hospital, Durham, NC; King's College Hospital, London, England; Guy's and St Thomas' Hospital, London, England; University College Hospital, London, England; Harefield Hospital, London, England; and Hertford County Hospital, Hertford, England.

References

1. Samei E, Ranger NT, Dobbins JT 3rd, Chen Y. Intercomparison of methods for image quality characterization. I. Modulation transfer function. *Med Phys* 2006;33:1454–1465.
2. Dobbins JT 3rd, Samei E, Ranger NT, Chen Y. Intercomparison of methods for image quality characterization. II. Noise power spectrum. *Med Phys* 2006;33:1466–1475.
3. Ranger NT, Samei E, Dobbins JT 3rd, Ravin CE. Assessment of detective quantum efficiency: intercomparison of a recently introduced international standard with prior methods. *Radiology* 2007;243:785–795.
4. International Electrotechnical Commission. Medical electrical equipment: characteristics of digital x-ray imaging devices. I. Determination of the detective quantum efficiency. Geneva, Switzerland: International Electrotechnical Commission, 2003.
5. Maidment AD, Albert M, Bunch PC, et al. Standardization of NPS measurements: interim report of AAPM TG16. In: Yaffe MJ, Antonuk LE, eds. *Proceedings of The International Society for Optical Engineering (SPIE): Medical imaging 2003—physics of medical imaging*. Vol 5030. Bellingham, Wash: SPIE, 2003; 523–532.
6. Illers H, Buhr E, Hoeschen C. Measurement of the detective quantum efficiency (DQE) of digital x-ray detectors according to the novel standard IEC 62220–1. *Radiat Prot Dosimetry* 2005;114:39–44.
7. Lawinski CP, Mackenzie A, Cole H, Blake P, Honey ID. Digital detectors for general radiography, a comparative technical report: report 05078, London, UK: Centre for Evidence-Based Purchasing, 2005.
8. Rivetti S, Lanconelli N, Campanini R, et al.

- Comparison of different commercial FFDM units by means of physical characterization and contrast-detail analysis. *Med Phys* 2006; 33:4198–4209.
9. Monnin P, Gutierrez D, Bulling S, Guntern D, Verdun FR. A comparison of the performance of digital mammography systems. *Med Phys* 2007;34:906–914.
 10. Muntz EP. Analysis of the significance of scattered radiation in reduced dose mammography, including magnification effects, scatter suppression, and focal spot and detector blurring. *Med Phys* 1979;6:110–117.
 11. Samei E. Performance of digital radiography detectors: factors affecting sharpness and noise. In: Samei E, Flynn MJ, eds. 2003; Syllabus: categorical course in diagnostic radiology physics—advances in digital radiography: digital radiographic display technologies. Oak Brook, Ill: Radiological Society of North America, 2003; 49–61.
 12. Kyprianou IS, Rudin S, Bednarek DR, Hoffmann KR. Generalizing the MTF and DQE to include x-ray scatter and focal spot unsharpness: application to a new microangiographic system. *Med Phys* 2005;32:613–626.
 13. Kyprianou IS, Rudin S, Bednarek DR, Hoffmann KR. Study of the generalized MTF and DQE for a new microangiographic system. In: Yaffe MJ, Flynn MJ, eds. Proceedings of The International Society for Optical Engineering (SPIE): medical imaging 2004—physics of medical imaging. Vol 5368. Bellingham, Wash: SPIE, 2004;349–360.
 14. Kyprianou IS, Ganguly A, Rudin S, Bednarek DR, Gallas BD, Myers KJ. Efficiency of the human observer compared with an ideal observer based on a generalized NEQ which incorporates scatter and geometric unsharpness: evaluation with a 2AFC experiment. In: Eckstein MP, Jiang Yulei, eds. Proceedings of The International Society for Optical Engineering (SPIE): medical imaging 2005;—image perception, observer performance, and technology assessment. Vol 5749. Bellingham, Wash: SPIE, 2005; 251–262.
 15. Yadava GK, Kyprianou IS, Rudin S, Bednarek DR, Hoffman KR. Generalized performance evaluation of x-ray image intensifier compared with a microangiographic system. In: Flynn MJ, ed. Proceedings of The International Society for Optical Engineering (SPIE): medical imaging 2005—physics of medical imaging. Vol 5745. Bellingham, Wash: SPIE, 2005;419–429.
 16. Shaw CC, Liu X, Lemacks M, Rong JX, Whitman GJ. Optimization of MTF and DQE in magnification radiography—a theoretical analysis. In: Dobbins JT 3rd, Boone JM, eds. Proceedings of The International Society for Optical Engineering (SPIE): medical imaging 2000—physics of medical imaging. Vol 3977. Bellingham, Wash: SPIE, 2000;467–475.
 17. Boyce SJ, Samei E. Imaging properties of digital magnification radiography. *Med Phys* 2006;33:984–996.
 18. Samei E, Ranger NT, MacKenzie A, Honey ID, Dobbins JT 3rd, Ravin CE. An experimental methodology to assess effective DQE (eDQE) of radiographic systems in the presence of scatter and magnification. *Med Phys* (in press, 2008).
 19. Conway BJ, Butler PF, Duff JE, et al. Beam quality independent attenuation phantom for estimating patient exposure from x-ray automatic exposure controlled chest examinations. *Med Phys* 1984;11:827–832.
 20. Food and Drug Administration and Conference of Radiation Control Program Directors. Nationwide evaluation of X-ray trends: twenty-five years of NEXT. Rockville, Md: US Food and Drug Administration, 2003.
 21. Flynn MJ, Samei E. Experimental comparison of noise and resolution for 2k and 4k storage phosphor radiography systems. *Med Phys* 1999;26:1612–1623.
 22. Samei E, Flynn MJ, Reimann DA. A method for measuring the presampled MTF of digital radiographic systems using an edge test device. *Med Phys* 1998;25:102–113.
 23. Floyd CE, Lo JY, Chotas HG, Ravin CE. Quantitative scatter measurement in digital radiography using a photostimulable phosphor imaging system. *Med Phys* 1991;18: 408–413.
 24. Samei E, Lo JY, Yoshizumi TT, et al. Comparative scatter and dose performance of slot-scan and full-field digital chest radiography systems. *Radiology* 2005;235:940–949.
 25. Mackenzie A, Honey ID. Characterization of noise sources for two generations of computed radiography systems using powder and crystalline photostimulable phosphors. *Med Phys* 2007;34:3345–3357.
 26. Samei E, Saunders RS, Lo JY, et al. Fundamental imaging characteristics of a slot-scan digital chest radiographic system. *Med Phys* 2004;31:2687–2698.
 27. Samei E, Flynn MJ. An experimental comparison of detector performance for direct and indirect digital radiography systems. *Med Phys* 2003;30:608–622.
 28. Sorenson JA, Floch J. Scatter rejection by air gaps: an empirical model. *Med Phys* 1985;12:308–316.
 29. Persliden J, Carlsson GA. Scatter rejection by air gaps in diagnostic radiology: calculations using a Monte Carlo collision density method and consideration of molecular interference in coherent scattering. *Phys Med Biol* 1997;42:155–175.

Radiology 2008

This is your reprint order form or pro forma invoice

(Please keep a copy of this document for your records.)

Reprint order forms and purchase orders or prepayments must be received 72 hours after receipt of form either by mail or by fax at 410-820-9765. It is the policy of Cadmus Reprints to issue one invoice per order.

Please print clearly.

Author Name _____
Title of Article _____
Issue of Journal _____ Reprint # _____ Publication Date _____
Number of Pages _____ KB # _____ Symbol Radiology
Color in Article? Yes / No (Please Circle)

Please include the journal name and reprint number or manuscript number on your purchase order or other correspondence.

Order and Shipping Information

Reprint Costs (Please see page 2 of 2 for reprint costs/fees.)

_____ Number of reprints ordered \$ _____
_____ Number of color reprints ordered \$ _____
_____ Number of covers ordered \$ _____
Subtotal \$ _____
Taxes \$ _____

(Add appropriate sales tax for Virginia, Maryland, Pennsylvania, and the District of Columbia or Canadian GST to the reprints if your order is to be shipped to these locations.)

First address included, add \$32 for
each additional shipping address \$ _____

TOTAL \$ _____

Shipping Address (cannot ship to a P.O. Box) Please Print Clearly

Name _____
Institution _____
Street _____
City _____ State _____ Zip _____
Country _____
Quantity _____ Fax _____
Phone: Day _____ Evening _____
E-mail Address _____

Additional Shipping Address* (cannot ship to a P.O. Box)

Name _____
Institution _____
Street _____
City _____ State _____ Zip _____
Country _____
Quantity _____ Fax _____
Phone: Day _____ Evening _____
E-mail Address _____

* Add \$32 for each additional shipping address

Payment and Credit Card Details

Enclosed: Personal Check _____
Credit Card Payment Details _____
Checks must be paid in U.S. dollars and drawn on a U.S. Bank.
Credit Card: VISA Am. Exp. MasterCard
Card Number _____
Expiration Date _____
Signature: _____

Please send your order form and prepayment made payable to:

Cadmus Reprints
P.O. Box 751903
Charlotte, NC 28275-1903

*Note: Do not send express packages to this location, PO Box.
FEIN #:541274108*

Signature _____
Signature is required. By signing this form, the author agrees to accept the responsibility for the payment of reprints and/or all charges described in this document.

Invoice or Credit Card Information

Invoice Address Please Print Clearly

Please complete Invoice address as it appears on credit card statement

Name _____
Institution _____
Department _____
Street _____
City _____ State _____ Zip _____
Country _____
Phone _____ Fax _____
E-mail Address _____

**Cadmus will process credit cards and Cadmus Journal
Services will appear on the credit card statement.**

*If you don't mail your order form, you may fax it to 410-820-9765 with
your credit card information.*

Radiology 2008

Black and White Reprint Prices

Domestic (USA only)						
# of Pages	50	100	200	300	400	500
1-4	\$221	\$233	\$268	\$285	\$303	\$323
5-8	\$355	\$382	\$432	\$466	\$510	\$544
9-12	\$466	\$513	\$595	\$652	\$714	\$775
13-16	\$576	\$640	\$749	\$830	\$912	\$995
17-20	\$694	\$775	\$906	\$1,017	\$1,117	\$1,220
21-24	\$809	\$906	\$1,071	\$1,200	\$1,321	\$1,471
25-28	\$928	\$1,041	\$1,242	\$1,390	\$1,544	\$1,688
29-32	\$1,042	\$1,178	\$1,403	\$1,568	\$1,751	\$1,924
Covers	\$97	\$118	\$215	\$323	\$442	\$555

Color Reprint Prices

Domestic (USA only)						
# of Pages	50	100	200	300	400	500
1-4	\$223	\$239	\$352	\$473	\$597	\$719
5-8	\$349	\$401	\$601	\$849	\$1,099	\$1,349
9-12	\$486	\$517	\$852	\$1,232	\$1,609	\$1,992
13-16	\$615	\$651	\$1,105	\$1,609	\$2,117	\$2,624
17-20	\$759	\$787	\$1,357	\$1,997	\$2,626	\$3,260
21-24	\$897	\$924	\$1,611	\$2,376	\$3,135	\$3,905
25-28	\$1,033	\$1,071	\$1,873	\$2,757	\$3,650	\$4,536
29-32	\$1,175	\$1,208	\$2,122	\$3,138	\$4,162	\$5,180
Covers	\$97	\$118	\$215	\$323	\$442	\$555

International (includes Canada and Mexico)						
# of Pages	50	100	200	300	400	500
1-4	\$272	\$283	\$340	\$397	\$446	\$506
5-8	\$428	\$455	\$576	\$675	\$784	\$884
9-12	\$580	\$626	\$805	\$964	\$1,115	\$1,278
13-16	\$724	\$786	\$1,023	\$1,232	\$1,445	\$1,652
17-20	\$878	\$958	\$1,246	\$1,520	\$1,774	\$2,030
21-24	\$1,022	\$1,119	\$1,474	\$1,795	\$2,108	\$2,426
25-28	\$1,176	\$1,291	\$1,700	\$2,070	\$2,450	\$2,813
29-32	\$1,316	\$1,452	\$1,936	\$2,355	\$2,784	\$3,209
Covers	\$156	\$176	\$335	\$525	\$716	\$905

International (includes Canada and Mexico))						
# of Pages	50	100	200	300	400	500
1-4	\$278	\$290	\$424	\$586	\$741	\$904
5-8	\$429	\$472	\$746	\$1,058	\$1,374	\$1,690
9-12	\$604	\$629	\$1,061	\$1,545	\$2,011	\$2,494
13-16	\$766	\$797	\$1,378	\$2,013	\$2,647	\$3,280
17-20	\$945	\$972	\$1,698	\$2,499	\$3,282	\$4,069
21-24	\$1,110	\$1,139	\$2,015	\$2,970	\$3,921	\$4,873
25-28	\$1,290	\$1,321	\$2,333	\$3,437	\$4,556	\$5,661
29-32	\$1,455	\$1,482	\$2,652	\$3,924	\$5,193	\$6,462
Covers	\$156	\$176	\$335	\$525	\$716	\$905

Minimum order is 50 copies. For orders larger than 500 copies, please consult Cadmus Reprints at 800-407-9190.

Reprint Cover

Cover prices are listed above. The cover will include the publication title, article title, and author name in black.

Shipping

Shipping costs are included in the reprint prices. Domestic orders are shipped via UPS Ground service. Foreign orders are shipped via a proof of delivery air service.

Multiple Shipments

Orders can be shipped to more than one location. Please be aware that it will cost \$32 for each additional location.

Delivery

Your order will be shipped within 2 weeks of the journal print date. Allow extra time for delivery.

Tax Due

Residents of Virginia, Maryland, Pennsylvania, and the District of Columbia are required to add the appropriate sales tax to each reprint order. For orders shipped to Canada, please add 7% Canadian GST unless exemption is claimed.

Ordering

Reprint order forms and purchase order or prepayment is required to process your order. Please reference journal name and reprint number or manuscript number on any correspondence. You may use the reverse side of this form as a proforma invoice. Please return your order form and prepayment to:

Cadmus Reprints
P.O. Box 751903
Charlotte, NC 28275-1903

Note: Do not send express packages to this location, PO Box. FEIN #: 541274108

Please direct all inquiries to:

Rose A. Baynard
800-407-9190 (toll free number)
410-819-3966 (direct number)
410-820-9765 (FAX number)
baynardr@cadmus.com (e-mail)

Reprint Order Forms and purchase order or prepayments must be received 72 hours after receipt of form.